

## METHODS

# Postcranial skeletal pneumaticity: a case study in the use of quantitative microCT to assess vertebral structure in birds

R. J. Fajardo,<sup>1</sup> E. Hernandez<sup>1,2</sup> and P. M. O'Connor<sup>3</sup>

<sup>1</sup>Orthopedic Biomechanics Laboratory, Beth Israel Deaconess Medical Center and Harvard Medical School, Boston, MA, USA

<sup>2</sup>Department of Anthropology, Boston University, Boston, MA, USA

<sup>3</sup>Department of Biomedical Sciences, Ohio University College of Osteopathic Medicine, Athens, Ohio, USA

## Abstract

Limb elements in birds have been characterized as exhibiting a reduction in trabecular bone, thinner cortices and decreased bending strength when pneumatized, yet it is unclear if these characteristics generalize to the axial skeleton. Thin section techniques, the traditional gold standard for bone structure studies, have most commonly been applied to the study of avian bone. This destructive technique, however, makes it impossible subsequently to use the same samples in experimental testing systems that allow researchers to correlate structure with the mechanical properties of the bone. Micro-computed tomography ( $\mu$ CT), a non-destructive X-ray imaging technique, can be used to assess the effect of pneumatization on vertebral cortical and trabecular bone through virtual extraction and structural quantification of each tissue type. We conducted a preliminary investigation of the application of  $\mu$ CT methods to the study of cortical and trabecular bone structure in a small sample of pneumatized and apneumatic thoracic vertebrae. The sample consisted of two similar-sized anatids, *Aix sponsa* ( $n = 7$ ) and *Oxyura jamaicensis* ( $n = 5$ ). Volumes of interest were created that contoured (outlined) the boundaries of the ventral cortical bone shell, the trabecular compartment and the whole centrum (cortical bone + trabecular bone), and allowed independent structural analysis of each volume of interest. Results indicated that bone volume fraction of the whole centrum was significantly higher in the apneumatic *O. jamaicensis* than in the pneumatized *A. sponsa* (*A. sponsa* = 36%, *O. jamaicensis* = 48%,  $P < 0.05$ ). In contrast, trabecular bone volume fraction was similar between the two species. The ventral cortical bone shell was approximately 23% thinner ( $P < 0.05$ ) in *A. sponsa* (0.133 mm) compared with apneumatic *O. jamaicensis* (0.172 mm). This case study demonstrates that  $\mu$ CT is a powerful non-destructive imaging technique that may be applied to the three-dimensional study of avian bone. The preliminary results suggest that pneumatic and apneumatic vertebrae of comparably sized avian species differ in relative bone volume, with the largest difference apparent at the level of the cortex, and not within trabecular bone. The presence of relatively thin cortices in pneumatic vertebrae is consistent with previous studies contrasting diaphyseal cortical bone between pneumatic and apneumatic long bones. Methodological issues related to this and any comparative  $\mu$ CT study of bone structure are discussed.

**Key words** Aves; comparative morphology; microcomputed tomography; pneumaticity; vertebral column.

## Correspondence



Dr Roberto José Fajardo, PhD, Orthopedic Biomechanics Laboratory, Beth Israel Deaconess Medical Center, 330 Brookline Ave., RN 115, Boston, MA 02215, USA. T: +1 617 667 4572; F: +1 617 667 7175; E: rfajardo@bidmc.harvard.edu

The first two authors contributed equally to the completion of this study.

Accepted for publication 12 April 2007

## Introduction

Pneumatization of the postcranial skeleton represents one of the hallmark adaptations characterizing living birds, a radiation that includes approximately 10 000 extant species. Postcranial skeletal pneumaticity results from the extension of pneumatic diverticula (epithelial

	J O A 7 4 9	Operator: Yu Yanjun		Dispatch: 15.05.07	PE: Graeme Henderson
Journal Name	Manuscript No.	Proofreader: Zhang Yeping	No. of Pages: 11	Copy-editor: Patrick Smith	

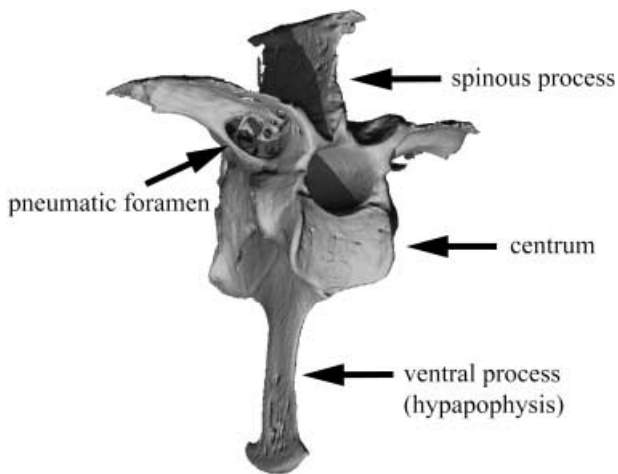


**Fig. 1** Three-dimensional reconstructed  $\mu$ CT image demonstrating the location of a pneumatic foramen and other features on a third thoracic vertebra (caudolateral view). The pneumatic foramen is an osteological indicator of pneumatization. Wood duck (*Aix sponsa*, MCZ 346926).

lined outpocketings) of the pulmonary air sacs and lungs throughout the marrow cavities. The development of the air sacs within the skeleton is generally acknowledged to occur after hatching (Locy & Larsell, 1916a,b; Bremer, 1940; Hogg, 1984b), although the precise mechanism by which this occurs remains enigmatic. The pneumatic foramen, an osteological correlate of pneumaticity, allows the passage of air sac diverticula through the cortical surface and into internal cavities within bone (Fig. 1; Crisp, 1857; O'Connor, 2004, 2006). The anatomical distribution of pneumatization throughout the postcranial skeleton varies both among and within different groups of birds (Crisp, 1857; King & Kelly, 1956; King, 1957; Bellairs & Jenkin, 1960; King & McLelland, 1979; O'Connor, 2004).

Continued interest exists in postcranial skeletal pneumatization and its effect on the structural and mechanical properties of avian bone (Currey & Alexander, 1985; Cubo & Casinos, 1998, 2000; Casinos & Cubo, 2001; O'Connor, 2004, 2006; de Margerie et al. 2005). Several studies have examined the structure of pneumatic long bones (Currey & Alexander, 1985; Cubo & Casinos, 1998, 2000; Casinos & Cubo, 2001; de Margerie et al. 2005). In particular, Currey & Alexander (1985) measured cortical thickness as the quantity  $K$ , the ratio of the internal to external diameter. These values were compared with a range of theoretical optima predicated on models of resistance to different types of loading environments, with results indicating that pneumatic bones are thinner

walled than marrow-filled bones and are not selected for heavy load bearing. Building upon this work, Cubo & Casinos (2000) examined structural and mechanical properties of pneumatic long bones, including cortical thickness, bending strength and Young's modulus. Their results indicate that pneumatic long bones have thinner cortices, reduced stiffness and less resistance to bending when compared with size-matched apneumatic bones.

The impact of pneumatization on the trabecular bone of long bones, not to mention components of the axial skeleton, has not been quantitatively assessed. The current understanding of pneumaticity in the vertebral column has been limited to regional anatomical descriptions (King & Kelly, 1956; King, 1957; Hogg, 1984a; O'Connor, 2004). Moreover, there are no published studies comparing the bone microstructure of pneumatic and marrow-filled vertebrae. Because cortical and trabecular bone work synergistically to determine bone strength (Rogers & LaBarbara, 1993; Lotz et al. 1995; Silva et al. 1997; Grynpsas et al. 2000), it is of interest to examine the effect of pneumatization on these bone tissue types.

Previous studies have used destructive sectioning methods to assess bone structure. Sectioning methods are the gold standard for assessing cancellous and cortical bone structure in comparative avian bone studies (Meister, 1962; Currey & Alexander, 1985; Cubo & Casinos, 2000; Horner et al. 2000; de Margerie et al. 2005). Micro-computed tomography ( $\mu$ CT) is a high-resolution X-ray imaging technique (Rüeggsegger et al. 1996) initially developed for, and now commonly used in, orthopaedic research to assess cancellous and cortical bone structure. Moreover, it is becoming a common approach in studies of comparative primate morphology research since its original introduction (Fajardo & Müller, 2001; MacLachy & Müller, 2002; Ryan & Ketcham, 2002a,b, 2005; Ryan & van Rietbergen, 2005; Maga et al. 2006; Fajardo et al. 2007). One advantage of the  $\mu$ CT method is that it is non-destructive and as a result specimens may subsequently be used in either soft tissue histology or mechanical testing. The latter is important because it is ideal directly to correlate structure and mechanical properties in the same specimens. Another advantage is that all structural measurements are completed in a three-dimensional (3D) volume, circumventing many of the structural assumptions about trabecular bone (Parfitt et al. 1983) and stereology-related caveats (Underwood, 1970; Weibel, 1979, 1980) pertinent to 2D morphometry. Also, in many  $\mu$ CT systems, the image

files can be manipulated to extract the 3D volume of cancellous and/or cortical bone in a vertebra (or any bone where the two tissues are adjacent) and quantify their structure independently.

We present a methodological case study to assess the application of  $\mu$ CT to investigations of the effect of pneumatization on the whole bone structural properties of avian vertebrae. Morphometric results were compared with previous studies examining the effect of pneumatization on elements of the appendicular skeleton.

## Materials and methods

The third thoracic vertebrae of two species of ducks (Anseriformes: Anatidae) were used for comparisons of structural properties between pneumatic and apneumatic vertebrae. All samples were borrowed from collections at the American Museum of Natural History (AMNH), the Museum of Comparative Zoology at Harvard University (MCZ), and the Yale University Peabody Museum of Comparative Zoology (YPM).

The sample consisted of 12 adult male specimens, including seven *Aix sponsa* (wood duck) and five *Oxyura jamaicensis* (ruddy duck). These represent closely related species within the family Anatidae (Livezey, 1997), characterized by similar body masses (*Aix sponsa* = 658 g and *Oxyura jamaicensis* = 554 g, Dunning, 1993), but differing pneumaticity states. The thoracic vertebral

column of *A. sponsa* is pneumatized whereas that of *O. jamaicensis* is not (O'Connor, 2004). These species also differ in aspects of their behavioural repertoire, with *A. sponsa* as a generalized dabbling duck and *O. jamaicensis* representing a dedicated diving species.

## $\mu$ CT imaging

Three-dimensional reconstructions of the third thoracic vertebrae were obtained using a  $\mu$ CT system ( $\mu$ CT-40; Scanco Medical AG). Müller et al. (1998) demonstrated that such systems accurately reflect bone microarchitecture through comparisons with thin section samples. Each vertebra was positioned in a cylindrical sample holder and secured using a synthetic foam mould. Scans were acquired with a 30-mm field of view, 55 kV,  $1024 \times 1024$ -pixel matrix, 0.030-mm slice thickness, and an integration time of 300 ms. These settings resulted in a 30- $\mu$ m isotropic voxel. A smaller field of view, which would have reduced the voxel size, could not be attained without sectioning the specimens.

Three volumes of interest (VOIs) were created to characterize vertebrae structurally, including (1) trabecular bone within the centrum, (2) cortical bone delimiting the centrum and (3) the whole centrum (including the trabecular and cortical bone). Each  $\mu$ CT scan produced a 3D stack that could be viewed slice by slice (Fig. 2a,b). Beginning ten slices caudal to the last visual evidence

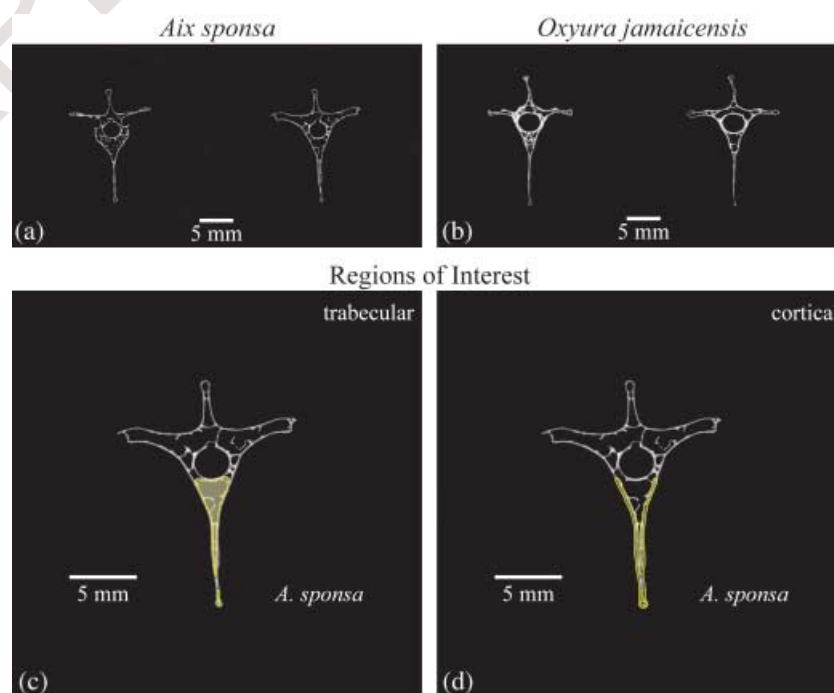


**Fig. 2** Two greyscale images from the slice stack of (a) *Aix sponsa* (MCZ 346926) and (b) *Oxyura jamaicensis* (AMNH 10690). Regions of interest (ROIs) were constructed to delimit the trabecular bone compartment (c) and the ventral cortical bone (d). (c) and (d) use a single image of *A. sponsa*. Index ROIs were established on every tenth slice with region of interest shape changes interpolated between the index slices. The combined slice stack (based on ROIs) was used to create a VOI for each specimen. In each region of interest the content (structure) of the green shaded region was measured.

of the cranial growth plate, we used a region of interest (ROI, which is a 2D area) drawing tool to outline either the marrow cavity, ventral cortical bone shell including the ventral process (hypapophysis) or the whole centrum (including the ventral process) in individual image slices. This process was repeated at every tenth slice through the vertebra until we reached a plane ten slices cranial to the caudal growth plate of the centrum. The ten-slice buffer from both growth plates was chosen to avoid the transitional zone between the trabecular bone and the porous endplate cortical bone in vertebrae. For the trabecular bone, ROI outlines followed the endosteal border of the vertebral centrum (Fig. 2c). The cortical bone ROI was constructed by outlining the periosteal and endosteal boundaries of the ventral cortical shell (Fig. 2d). The whole centrum ROI was constructed by outlining the periosteal boundaries of the centrum (including the ventral process) and a segment connecting the ventrolateral extent of each pedicle (following the periosteal contour of the vertebral canal). Finally, the  $\mu$ CT system's MORPH function used these index ROI slices to interpolate the shape changes of the ROIs between every tenth index slice and create VOIs. Each VOI was reviewed and any errors introduced by the computer interpolation algorithm were manually corrected.

Thresholding, or segmentation of an image, refers to the process of binarizing a data set in order to distinguish bone from the surrounding background. This process is non-trivial and can lead to measurement error if applied arbitrarily (Hara et al. 2002). We applied an adaptive, iterative threshold to distinguish bone from background in all images (detailed in Ridler & Calvard, 1978; Trussell, 1979; Ryan & Ketcham, 2002a; Meinel et al. 2005; Maga et al. 2006). Importantly, the precision, accuracy and stability of this approach have been tested on a variety of image types (Glasbey, 1993; Leung & Lam, 1996; Rajagopalan et al. 2005).

The following structural parameters were measured in three dimensions and without any model assumptions (Parfitt et al. 1983; Guldborg et al. 2003) or concern for caveats related to measurements in 2D sections (i.e. stereology; Underwood, 1970; Weibel, 1979, 1980). Trabecular bone volume fraction, Tb.BV/TV, is the relative amount of trabecular bone volume in the VOI. This is measured as the ratio of bone voxels to the total number of voxels. Trabecular thickness, Tb.Th, is an average measurement of the thickness of all trabeculae (Hildebrand & Rüegsegger, 1997; Hildebrand et al. 1999).

The average thickness represents the mean diameter of all non-overlapping spheres of maximum diameter positioned within the trabecular lattice (Hildebrand & Rüegsegger, 1997). Trabecular number, Tb.N, is a measure of the number of trabeculae per millimetre in 3D space (Hildebrand et al. 1999). This is calculated as the average inverse distance between the midline long axes of all trabeculae (Hildebrand et al. 1999). The structural degree of anisotropy, Tb.DA, is a 3D measurement based on bone structure orientation that follows the method described by Laib (2000). In brief, this calculation uses an orientation distribution calculated from surface normals of each triangle in a mesh framework projected onto the bone surface. These data are then fit to an ellipsoid using a least-squares approach and the DA is expressed as a ratio of the longest to shortest vector of the ellipsoid. A value of one indicates no preferred plane of structural orientation (isotropy), with values greater than one indicative of increasing organization of the lattice (anisotropy). The cortical thickness, Ct.Th, is measured using the same spheres approach described for Tb.Th above. Finally, the whole centrum bone volume fraction, Wh.BV/TV, is the ratio of all bone voxels (Tb. + Ct.) to the total number of voxels in the whole centrum VOI.

## Statistics

Means, standard deviations and coefficients of variation were calculated for all measurements. Independent *t*-tests and non-parametric equivalent tests were used to compare species means (significance threshold was set to  $\alpha = 0.05$ ). All statistical tests were performed in SPSS v. 8.0.

## Results

Table 1 lists the quantitative results of the structural analyses and Fig. 3 shows representative 3D reconstructions of the vertebrae. Tb.BV/TV and Tb.N were similar in *Aix sponsa* and *Oxyura jamaicensis*, but with *A. sponsa* possessing higher coefficients of variation in both measurements (32 and 34% in *A. sponsa* vs. 19 and 22% in *O. jamaicensis*, respectively). Tb.DA values were also similar in the two anatid species. By contrast, trabeculae were 11.5% thinner in *A. sponsa* (Tb.Th = 0.108 mm) than in *O. jamaicensis* (Tb.Th = 0.122). These means were significantly different in the *t*-test but not in the Wilcoxon non-parametric test. Ct.Th was significantly

1

**Table 1** Results of morphometric assessments of trabecular (Tb.), cortical (Ct.) and whole centrum (Wh.) volumes of interest. Means, standard deviations (SD) and coefficients of variation (CoV) are reported along with the results of the parametric and non-parametric statistical analyses. Coefficients of variation are presented as percentages

	<i>A. sponsa</i>	<i>O. jamaicensis</i>	t-test	Wilcoxon
Tb.BV/TV (%)	16.0	15.9	NS	NS
SD	5.2	3.1		
CoV (%)	32	19		
Tb.N (mm <sup>-1</sup> )	1.46	1.39	NS	NS
SD	0.49	0.30		
CoV (%)	34	22		
Tb.Th (mm)	0.108	0.122	$P < 0.05$	NS
SD	0.006	0.012		
CoV (%)	5	9		
Tb.DA (-)	1.36	1.34	NS	NS
SD	0.18	0.11		
CoV (%)	13	8		
Ct.Th (mm)	0.133	0.172	$P < 0.05$	$P < 0.05$
SD	0.007	0.049		
CoV (%)	6	28		
Wh.BV/TV (%)	35.8	48.1	$P < 0.05$	$P < 0.05$
SD	3.6	4.3		
CoV (%)	10	9		

thinner ( $P < 0.05$ ) in *A. sponsa* (Ct.Th = 0.133 mm) than in *O. jamaicensis* (Ct.Th = 0.172 mm). Figure 4 illustrates a colour-indexed cortical thickness distribution map in which the ventral cortex of *O. jamaicensis* contains several local regions of greater thickness than *A. sponsa*. Wh.BV/TV was significantly lower in *A. sponsa* than in *O. jamaicensis* (35% vs. 48%, respectively).

## Discussion

The two related objectives of this study were to (1) provide a preliminary examination of vertebral structure in pneumatic and apneumatic bone, and (2) evaluate the application of  $\mu$ CT approaches in avian comparative osteology. What follows is a brief overview of these results and their implications in addition to a discussion of methodological issues relevant for similar studies.

### The microstructure of pneumatic and apneumatic bone: a case study in duck vertebrae

Previous studies suggested that pneumatization of the avian postcranium is associated with trabecular degeneration occurring in conjunction with the spreading of air sac diverticula throughout the medullary space (Bremer, 1940; Bellairs & Jenkin, 1960). Contrary to expectations, trabecular bone volume fraction was similar in adult *Aix sponsa* (pneumatic) and *Oxyura jamaicensis* (apneumatic), suggesting that pneumatization is not associated with an overall decrease in trabecular bone. Although the average thickness of trabeculae was lower in *A. sponsa*, this did not result in a lower Tb.BV/TV than *O. jamaicensis* because Tb.N was slightly higher (absolutely) in *A. sponsa*. However, the average thickness of cortical bone was significantly lower (23%) in *A. sponsa* than in *O. jamaicensis*, a finding that accounts for the relative whole bone volume fraction differences observed between the two species. No other structural variables were significantly different between the species.

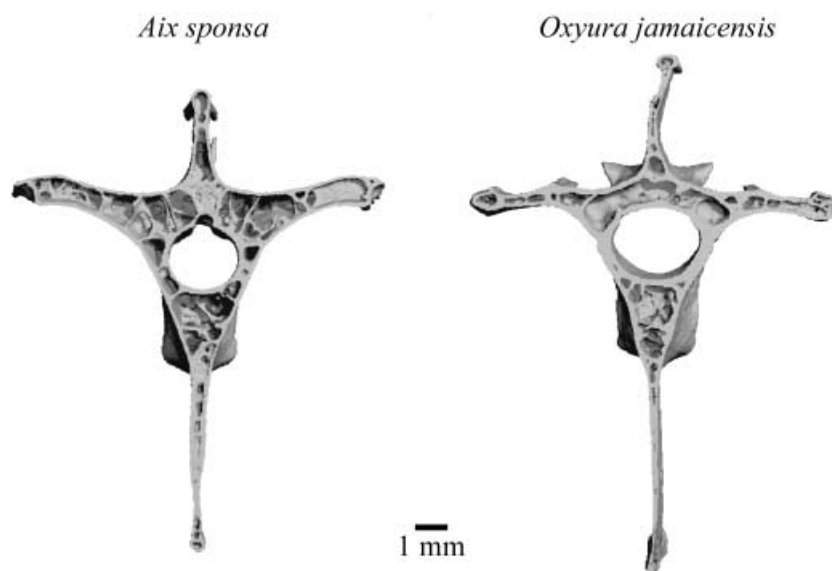


**Fig. 3** Three-dimensional reconstructions of the vertebrae of *Aix sponsa* and *Oxyura jamaicensis* with the cranial half of the VOI removed in order to view the internal bony architecture and cortical bone thickness.

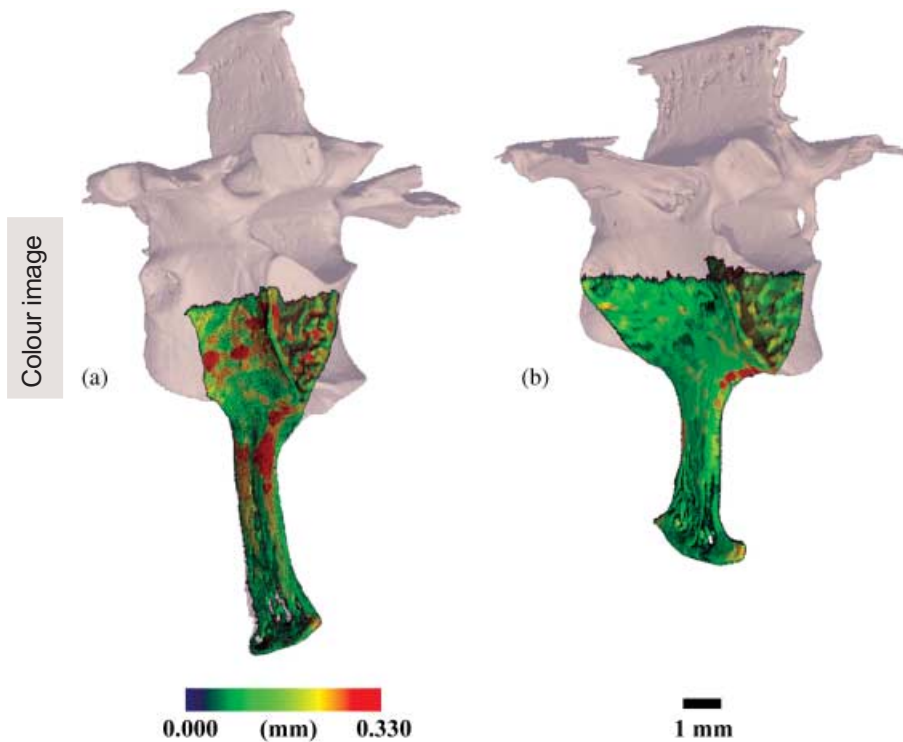


**Fig. 4** Three-dimensional coloured indexed renderings of the centrum VOI illustrating the distribution of cortical thickness measurements in (a) *Oxyura jamaicensis* (AMNH 10690) and (b) *Aix sponsa* (MCZ 346926). The thickness distribution is scaled to the highest local thickness measured in both species (0.330 mm, *O. jamaicensis*). Thickness distribution maps indicate that the cortical shell of *O. jamaicensis* has a wide range of cortical thickness throughout the ventral cortex, with several regions exhibiting higher thicknesses than the generally homogeneous thickness observed in *Aix sponsa*.

We also observed greater intraspecific variability in the trabecular bone volume fraction in the third thoracic vertebrae of *Aix sponsa*. The third thoracic vertebra was chosen because it was reported to be consistently pneumatized in model taxa (e.g. chickens, pigeons; King, 1957; Hogg, 1984a), and thus it was assumed that this would hold for the pneumatic taxon in this study. The intraspecific variation in BV/TV we report may be a local effect and not representative of adjacent levels or the entire axial skeleton. Nevertheless, these results are intriguing because they at least suggest that pneumatization, as a rule, does not lead to reduced trabecular bone volume fraction. Moreover, these results extend the reported pattern of thinner cortices in pneumatic long bones to a representative portion of the axial skeleton.

The structural differences identified in this study correlate with a divergence in behavioural characteristics between the two taxa. The foraging strategy of *Oxyura jamaicensis* consists of sustained diving during food acquisition whereas *Aix sponsa* practises dabbling (with only minimal diving; Hepp & Bellrose, 1995; Johnsgard & Carbonell, 1996). Diving birds possess numerous anatomical specializations related to underwater propulsion (e.g. caudally positioned hind limbs, elongation of individual hind limb elements; Raikow, 1970; McCracken

et al. 1999) and they also exhibit a reduction in postcranial pneumatization relative to non-divers, even among closely related taxa (O'Connor, 2004). The lack of aeration in dedicated diving taxa is typically explained on the grounds that the presence of air might limit the ability to forage under water successfully (i.e. the increased buoyancy may be energetically disadvantageous in performing such specialized locomotor behaviours). In addition, increased cortical thickness is characteristic of aquatic animals (Wall, 1983; Currey & Alexander, 1985). Currey & Alexander (1985) reported that long bones of aquatic tetrapods exhibit high density values, smaller marrow cavities, and thicker walls relative to terrestrial taxa, all of which work to minimize the amount of low-density fat contained within the medullary cavity. Wall (1983) also suggested that thick-walled bones are a means of achieving neutral buoyancy.

The high levels of intraspecific variability in trabecular bone volume fraction (and other variables) of *Aix sponsa* highlight an important set of study design challenges encountered, underlining a characteristic that others will need to consider. We restricted our samples to adult male skeletal material of unknown exact age, a fact that must be emphasized. At the moment, we cannot determine the source of the high intraspecific variability observed in the adult phenotype of *A. sponsa*. The

pneumatized adult avian skeletal phenotype most likely results from complex and competing processes. First, mammalian trabecular bone structure is known to increase in absolute volume and volume fraction ontogenetically (Nafei et al. 2000; Tanck et al. 2001; Wolschrijn & Weijs, 2004). However, potentially working synchronously against this growth is the expansion of pneumatic epithelium within a bone, the latter process representing one that might induce variable resorption from individual to individual (Crisp, 1857; Locy & Larsell, 1916a,b; Bremer, 1940; Bellairs & Jenkin, 1960; King & McLelland, 1979; Hogg, 1984a,b; O'Connor, 2004). Lastly, ageing-associated trabecular bone loss and structural changes (after skeletal maturity), such as those known to occur in mammals (Mosekilde, 1990; Kammerer et al. 1995; Brodt et al. 1999; Cerroni et al. 2000; Halloran et al. 2002; Filardi et al. 2004; Glatt & Bouxsein in press), most likely also impact the adult avian phenotype. In the future, it will be critical to examine how the ontogeny of bone growth, pneumatization and ageing-associated bone loss and structural changes in avian bone interact to determine the adult skeletal phenotype. In this study, only males were included in the sample to avoid any potential sex differences, particularly those related to reproduction (egg production). Sex-related differences may exist in aspects of the pneumatization process, the bone structure or both. Furthermore, it is known that egg-producing females lose cancellous bone in the metaphyses of long bones (Wilson & Thorp, 1998). Although data are lacking on this point in birds, it would not be surprising to discover that calcium stores in vertebral trabecular bone respond dynamically to egg production. It is interesting to note that vertebral trabecular bone turnover in mammals is equal to or greater than metaphyseal trabecular bone turnover (Lane et al. 1998; Nishida et al. 1998). In an ideal situation, researchers would control for age, gender, reproductive status, hormone levels and the state of health (Weaver & Chalmers, 1966; Parfitt et al. 1983; Kleerekoper et al. 1985; Fazzalari et al. 1992; Grote et al. 1995; Kalkwarf & Specker, 1995; Majumdar et al. 1997; Parsons et al. 1997; Lees & Jerome, 1998) but this is unrealistic in studies utilizing wild-collected specimens. More importantly, researchers should be aware that these factors may introduce variance into their study and it is to be hoped that others will embark on investigations to document the effects of age, sex and reproduction on the pneumatization process and bone structure.

### Methodological concerns of comparative $\mu$ CT studies

The  $\mu$ CT system allowed us to analyse the constituent elements of the vertebral centrum, including cortical and trabecular bone. Similar applications of  $\mu$ CT and its powerful VOI tools are used in orthopaedic research (e.g. Laib, 2000; Judex et al. 2004; Glatt & Bouxsein in press). Although X-ray microtomography has been used to visualize vascular networks in avian cortical bone (de Margerie et al. 2006), our work here is a novel application of the techniques to avian comparative bone structure. In the future, each working group will face a decision on how to determine VOIs such that it allows for the independent measurement of cortical and trabecular bone parameters. This is an important consideration given that the boundary between trabecular bone and cortical bone is not typically discrete. The nodes joining trabecular and cortical bone, as well as trabeculae, contribute local maxima to 3D measurements of cortical and trabecular bone thickness (see Chappard et al. 2005). Our approach in delimiting cortical bone is to split these cortical–trabecular bone transition nodes in half in an effort to limit their influence on either cortical or trabecular bone analyses. Notably, these represent actual structures that contribute to bone integrity and are not just artefacts of the visualization process. We are confident that this approach is reasonable and that our cortical bone results (including the thickness colour map shown in Fig. 4) are representative of actual structural differences between the two species (Fig. 5).

The ventral cortical shell was included in this study as it is a mechanically relevant region due to the probable combined compressive and bending loads placed on

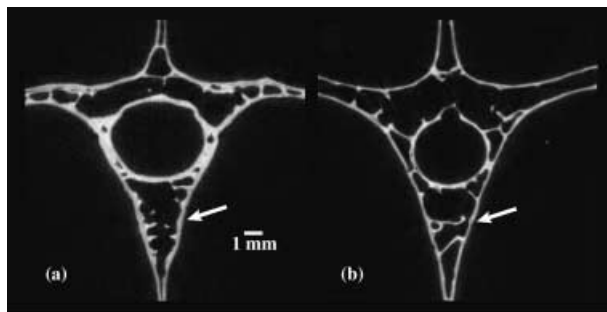


**Fig. 5** Greyscale images of (a) *Oxyura jamaicensis* and (b) *Aix sponsa* emphasizing relative cortical bone thicknesses in vertebrae. Specimens shown are the same as in Fig. 4. As demonstrated by the morphometric results, cortical bone is relatively thicker in *O. jamaicensis* (white arrows).

the vertebrae at this level. In addition, we chose to include the cortical shell of the hypapophysis in the analysis because it is continuous with the cortical shell of the centrum and the trabecular medullary cavity, and finally, it is lined by the pneumatic epithelium. In future studies comprising larger interspecific data sets it may be advantageous to increase the scope of the VOIs to assess more inclusively the structure of the entire cortical bone shell. Nonetheless, the fact that the results presented herein are consistent (i.e. relatively thin cortices in pneumatic bone) with analyses of diaphyseal bone indicates that the results are not purely an artefact of VOI definition.

Matters of scale are also important considerations in  $\mu$ CT studies. Such issues arise with regard to the selection of appropriate scan settings (resolution) and VOI determination. Specimens in the current study were scanned using a 30- $\mu$ m isotropic voxel, which represented at most 33% of the thickness of the average trabecula and a smaller percentage of the average cortical thickness. As vertebrae used in this study were of generally similar dimensions, all specimens were scanned with the same voxel size setting. Moreover, the use of a voxel size to trabecular thickness ratio of 33% falls within acceptable standards for quantifying both cortical and trabecular bone parameters. Müller et al. (1996, 1998) demonstrated that human vertebral trabecular bone, which is only slightly thicker than the trabeculae measured here, could be accurately quantified with 40- $\mu$ m isotropic voxels. However, in future studies that include more and smaller species, it may be necessary to reduce voxel size in the event that trabecular thickness scales with body mass. Studies conducted on mammals indicate that average trabecular thicknesses do not vary greatly in medium- to large-bodied taxa (Mullender et al. 1996; Swartz et al. 1998); however, some data suggest that smaller-bodied mammals (e.g. strepsirrhine primates) may in fact exhibit isometric relationships with regard to trabecular thickness (at least within a certain body size range; Fajardo et al. 2005). Although comparable data are not yet available for avian taxa, workers should at least be aware of such possibilities and attempt to scale voxel sizes so as to maintain a low voxel to trabecular thickness ratio, thereby reducing measurement error (e.g. Ryan & Ketcham, 2002a; Fajardo et al. 2005).

VOIs in this study were adjusted (scaled) for centrum height by using the first and last slice relative to the position of growth plates identified in the scan data

set. In studies of long bone metaphyseal regions, where VOI determination is a non-trivial matter, it is imperative that researchers consider adjusting VOIs relative to body size or some local, biomechanically relevant feature. For example, if uniform VOIs are applied across a set of species ranging in body size or long bone lengths, over-sampling may occur in smaller taxa (or undersampling in large taxa). Ultimately, this could undermine comparisons of biomechanically similar volumes and potentially conflate variation as intra-individual trabecular architectural variation in birds may, at least, be as high as that reported in humans and non-human primates (Whitehouse, 1974; Whitehouse & Dyson, 1974; Banse et al. 2001; Ryan & Ketcham, 2002a; Fajardo et al. 2007). As the goal of comparative cortical and trabecular bone studies is to analyse biomechanically homologous regions, VOIs must be scaled appropriately.

In conclusion, this study suggests that  $\mu$ CT-based methods represent a novel and useful tool for examining the effects of pneumatization on skeletal structure in birds. Based on data derived from two closely related, yet ecologically divergent, duck species, it appears that cortical bone is affected more than trabecular bone by the pneumatization process. Importantly,  $\mu$ CT provides a useful non-destructive means for assessing bone microstructure, a fact that will facilitate future studies encompassing larger comparative (i.e. interspecific) samples, not to mention research incorporating vertebrae from other regions of the axial skeleton. Moreover, future analyses may use the same specimens for mechanical testing while at the same time converting the voxel-based image data sets into finite element models (Van Rietbergen et al. 1999, 2003; Ryan & van Rietbergen, 2005). Such efforts will allow us to investigate directly the mechanical consequences of structural (and tissue mineral density) differences in pneumatic and apneumatic bone, whereas finite element models will aid investigations of load sharing between cortical and trabecular bone and the role played by these two tissue types in subarticular regions (see Currey, 2002). In closing, as it is generally appreciated that pneumatization occurs after hatching (Bremer, 1940; Hogg, 1984b), we are currently developing protocols to examine ontogenetic effects of pneumatization by comparing growth series of pneumatic and apneumatic species. Generally, this will allow us to document interactions between skeletal and respiratory tissues, and perhaps more importantly, to characterize tissue-level dynamics as pneumatic epithelium induces resorption and invades



bone. To this end, the advent of *in vivo*  $\mu$ CT systems may facilitate longitudinal ontogenetic studies of the pneumatization process that circumvent interindividual variability currently inherent in cross-sectional studies.

## Acknowledgements

We thank the Orthopedic Biomechanics Laboratory and its members for their assistance and support during the completion of this research and the preparation of this manuscript. For access to specimens, we thank the following individuals: M. and W. Smith at the Sweetbriar Nature Center, Long Island, NY; J. Trimble at the Harvard Museum of Natural History in Cambridge, MA; K. Zyskowski at the Yale Peabody Museum of Comparative Zoology in New Haven, CT; and P. Sweet at the American Museum of Natural History, New York. Lastly, this study was supported by the Department of Anthropology at Boston University, a grant from the Undergraduate Research Opportunities Program at Boston University, the Ohio University College of Osteopathic Medicine, and the Ohio University Office of Research and Sponsored Programs.

## References

- Banse X, Devogelaer JP, Munting E, Delloye C, Cornu O, Grynpas M (2001) Inhomogeneity of human vertebral cancellous bone: systematic density and structure patterns inside the vertebral body. *Bone* **28**, 563–571.
- Bellairs AA, Jenkin CR (1960) The skeleton of birds. In *Biology and Comparative Physiology of Birds* (ed. Marshall JA), pp. 241–300. New York: Academic Press.
- Bremer JL (1940) The pneumatization of the humerus in the common fowl and the associated activity of theelin. *Anat Rec* **77**, 197–211.
- Brodt MD, Ellis CB, Silva MJ (1999) Growing C57Bl/6 mice increase whole bone mechanical properties by increasing geometric and material properties. *J Bone Miner Res* **14**, 2159–2166.
- Casinos A, Cubo J (2001) Avian long bones, flight and bipedalism. *Comp Biochem Physiol Part A* **131**, 159–167.
- Cerroni AM, Tomlinson GA, Turnquist JE, Grynpas MD (2000) Bone mineral density, osteopenia, and osteoporosis in the *Rhesus macaques* of Cayo Santiago. *Am J Phys Anthropol* **113**, 389–410.
- Chappard D, Retailleau-Gaborit N, Legrand E, Basle MF, Audran M (2005) Comparison insight bone measurements by histomorphometry and microCT. *J Bone Miner Res* **20**, 1177–1184.
- Crisp E (1857) On the presence or absence of air in the bones of birds. *Proc Zool Soc Lond* **1857**, 215–220.
- Cubo J, Casinos A (1998) Biomechanical significance of cross-sectional geometry of avian long bones. *Eur J Morph* **36**, 19–28.
- Cubo J, Casinos A (2000) Incidence and mechanical significance of pneumatization in the long bones of birds. *Zool J Linn Soc* **130**, 499–510.
- Currey JD, Alexander RM (1985) The thickness of the walls of tubular bones. *J Zool, London* **206A**, 453–468.
- Currey JD (2002) *Bones: Structure and Mechanics*. Princeton, NJ: Princeton University Press.
- Dunning JB (1993) *CRC Handbook of Avian Body Masses*. Boca Raton, FL: CRC Press.
- Fajardo RJ, Müller R (2001) Three-dimensional analysis of nonhuman primate trabecular architecture using micro-computed tomography. *Am J Phys Anthropol* **115**, 327–336.
- Fajardo RJ, De Silva JM, Maclatchy LM, Bouxsein ML (2005) Relationships between body weight and vertebral bone architecture in primates that exhibit a 48-fold range in body weight. *Bone* **36**, S380–S380.
- Fajardo RJ, Müller R, Ketcham RA, Colbert M (2007) Nonhuman anthropoid primate femoral neck trabecular architecture and its relationship to locomotor mode. *Anat Rec A Discov Mol Cell Evol Biol* **290**, 422–436.
- Fazzalari NL, Moore RJ, Manthey BA, Vernon-Roberts B (1992) Comparative study of iliac crest and subchondral femoral bone in osteoarthritic patients. *Bone* **13**, 331–335.
- Filardi S, Zebaze RM, Duan Y, Edmonds J, Beck T, Seeman E (2004) Femoral neck fragility in women has its structural and biomechanical basis established by periosteal modeling during growth and endocortical remodeling during aging. *Osteoporos Int* **15**, 103–107.
- Glasbey CA (1993) An analysis of histogram-based thresholding algorithms. *Cvqip-Graph Mod Image Proc* **55**, 532–537.
- Glatt V, Bouxsein ML (in press) Age-related changes in trabecular architecture differ in female and male mice. *J Bone Miner Res*.
- Grote HJ, Amling M, Vogel M, Hahn M, Posl M, Delling G (1995) Intervertebral variation in trabecular microarchitecture throughout the normal spine in relation to age. *Bone* **16**, 301–308.
- Grynpas MD, Chachra D, Lundon K (2000) Bone quality in animal models of osteoporosis. *Drug Dev Res* **49**, 146–158.
- Guldborg RE, Ballock RT, Boyan BD, et al. (2003) Analyzing bone, blood vessels, and biomaterials with microcomputed tomography. *IEEE Eng Med Biol* **22**, 77–83.
- Halloran BP, Ferguson VL, Simske SJ, Burghardt A, Venton LL, Majumdar S (2002) Changes in bone structure and mass with advancing age in the male C57BL/6J mouse. *J Bone Miner Res* **17**, 1044–1050.
- Hara T, Tanck E, Homminga J, Huiskes R (2002) The influence of microcomputed tomography threshold variations on the assessment of structural and mechanical trabecular bone properties. *Bone* **31**, 107–109.
- Hepp GR, Bellrose FC (1995) Wood duck (*Aix sponsa*). In *The Birds of North America* (eds Gill AP). Philadelphia: The Academy of Natural Sciences and Washington, DC: The American Ornithologists' Union.
- Hildebrand T, Müller R, Laib A, Dequeker J, Rügsegger P (1999) Direct three-dimensional morphometric analysis of human cancellous bone: a microstructural data from spine, femur, ilia crest, and calcaneus. *J Bone Miner Res* **14**, 1167–1174.
- Hildebrand T, Rügsegger P (1997) A new method for the model-independent assessment of thickness in three-dimensional images. *J Microsc* **185**, 67–75.

- Hogg DA** (1984a) The distribution of pneumatization in the skeleton of the adult domestic fowl. *J Anat* **138**, 617–629.
- Hogg DA** (1984b) The development of pneumatization in the postcranial skeleton of the domestic fowl. *J Anat* **139**, 105–113.
- Horner JR, de Ricqlès A, Padian K** (2000) Long bone histology of the hadrosaurid dinosaur *Maiasaura peeblesorum*: growth dynamics and physiology based on an ontogenetic series of skeletal elements. *J Vert Paleont* **20**, 115–129.
- Johnsgard P, Carbonell M** (1996) *Ruddy Ducks and Other Stiffetails: Their Behavior and Biology*. Norman, OK: University of Oklahoma Press.
- Judex S, Garman R, Squire M, Busa B, Donahue LR, Rubin C** (2004) Genetically linked site-specificity of disuse osteoporosis. *J Bone Miner Res* **19**, 607–613.
- Kalkwarf HJ, Specker BL** (1995) Bone mineral loss during lactation and recovery after weaning. *Obstet Gynecol* **86**, 26–32.
- Kammerer CM, Sparks ML, Rogers J** (1995) Effects of age, sex and heredity on measures of bone mass in baboons (*Papio hamadryas*). *J Med Primatol* **24**, 236–242.
- King AS, Kelly DF** (1956) The aerated bones of *Gallus domesticus*: the fifth thoracic vertebra and sternal ribs. *Br Vet J* **112**, 279–283.
- King AS** (1957) The aerated bones of *Gallus domesticus*. *Acta Anat* **31**, 220–230.
- King AS, McLelland J** (1979) *Form and Function in Birds*. London: Academic Press.
- Kleerekoper M, Villanueva AR, Stanciu J, Sudhaker Rao D, Parfitt AM** (1985) The role of three-dimensional trabecular microstructure in the pathogenesis of vertebral compression fractures. *Calcif Tissue Int* **37**, 594–597.
- Laib A** (2000) 3D micro-computed tomography of trabecular and cortical bone architecture with application to a rat model of immobilisation osteoporosis. *Med Biol Eng Comput* **38**, 326–332.
- Lane NE, Thompson JM, Haupt D, Kimmel DB, Modin G, Kinney JH** (1998) Acute changes in trabecular bone connectivity and osteoclast activity in the ovariectomized rat in vivo. *J Bone Miner Res* **13**, 229–236.
- Lees CJ, Jerome CP** (1998) Effects of pregnancy and lactation on bone in *Cynomolgus* macaques: histomorphometric analysis of iliac biopsies. *Bone* **22**, 545–549.
- Leung CK, Lam FK** (1996) Performance analysis for a class of iterative image thresholding algorithms. *Pattern Rec* **29**, 1523–1530.
- Livezey BC** (1997) A phylogenetic classification of waterfowl (Aves: Anseriformes), including selected fossil species. *Ann Carn Mus* **66**, 457–496.
- Locy WA, Larsell O** (1916a) The embryology of the bird's lung based on observations of the domestic fowl. Part I. *Am J Anat* **19**, 1–44.
- Locy WA, Larsell O** (1916b) The embryology of the bird's lung based on observations of the domestic fowl. Part II. *Am J Anat* **20**, 447–504.
- Lotz JC, Cheal EJ, Hayes WC** (1995) Stress distributions within the proximal femur during gait and falls: implications for osteoporotic fracture. *Osteoporosis Int* **5**, 252–261.
- MaLatchy L, Müller R** (2002) A comparison of the femoral head and neck trabecular architecture of *Galago* and *Pero-dicticus* using micro-computed tomography ( $\mu$ CT). *J Human Evol* **43**, 89–105.
- Maga M, Kappelman J, Ryan TM, Ketcham RA** (2006) Preliminary observations on the calcaneal trabecular microarchitecture of extant large-bodied hominoids. *Am J Phys Anthropol* **129**, 410–417.
- Majumdar S, Genant HK, Grampp S, et al.** (1997) Correlation of trabecular bone structure with age, bone mineral density, and osteoporotic status: in vivo studies in the distal radius using high resolution magnetic resonance imaging. *J Bone Miner Res* **12**, 111–118.
- de Margerie E, Sanchez S, Cubo J, Castanet J** (2005) Torsional resistance as a principal component of the structural design of long bones: comparative multivariate evidence in birds. *Anat Rec A Discov Mol Cell Evol Biol* **282**, 49–66.
- de Margerie E, Tafforeau P, Rakotomanana L** (2006) In silico evolution of functional morphology: a test on bone tissue biomechanics. *JR Soc Interface* **3**, 679–687.
- McCracken KG, Harshman J, McClellan DA, Afton AD** (1999) Data set incongruence and correlated character evolution: an example of functional convergence in the hind-limbs of stiff-tail diving ducks. *Syst Biol* **48**, 683–714.
- Meinel L, Fajardo R, Hofmann S, et al.** (2005) Silk implants for the healing of critical size bone defects. *Bone* **37**, 688–698.
- Meister W** (1962) Histological structure of the long bones of penguins. *Anat Rec* **143**, 377–386.
- Mosekilde L** (1990) Age-related loss of vertebral trabecular bone mass and structure-biomechanical consequences. In *Biomechanics of Diarthrodial Joints* (eds Mow VC, Ratcliffe A, Woo S), pp. 83–96. Berlin: Springer.
- Mullender MG, Huiskes R, Versleyen H, Buma P** (1996) Osteocyte density and histomorphometric parameters in cancellous bone of the proximal femur in five mammalian species. *J Orthop Res* **14**, 972–979.
- Müller R, Koller B, Hildebrand T, Laib A, Gionollini S, Rügsegger P** (1996) Resolution dependency of microstructural properties of cancellous bone based on three-dimensional  $\mu$ -tomography. *Technol Health Care* **4**, 113–119.
- Müller R, Van Campenhout H, Van Damme B, et al.** (1998) Morphometric analysis of human bone biopsies: a quantitative structural comparison of histological sections and micro-computed tomography. *Bone* **23**, 59–66.
- Nafei A, Kabel J, Odgaard A, Linde F, Hvid I** (2000) Properties of growing trabecular ovine bone – Part II: Architectural and mechanical properties. *J Bone Joint Surg – Br Vol* **82B**, 921–927.
- Nishida S, Okimoto N, Okazaki Y, et al.** (1998) Effect of monoclonal anti-human gp130 antibody (GPX7) on bone turnover in normal and ovariectomized rats. *Calcif Tissue Int* **62**, 227–236.
- O'Connor PM** (2004) Pulmonary pneumaticity in the postcranial skeleton of extant Aves: a case study examining Anseriformes. *J Morph* **261**, 141–161.
- O'Connor PM** (2006) Postcranial pneumaticity: an evaluation of soft-tissue influences on the postcranial skeleton and the reconstruction of pulmonary anatomy in archosaurs. *J Morph* **267**, 1199–1226.
- Parfitt AM, Mathews CHE, Villanueva AR, Kleerekoper M, Frame B, Rao DS** (1983) Relationships between surface, volume, and thickness of iliac trabecular bone in aging and osteoporosis. *J Clin Invest* **72**, 1396–1409.

- Parsons TJ, van Dusseldorp M, van der Vliet M, van de Werken K, Schaafsma G, van Staveren W** (1997) Reduced bone mass in Dutch adolescents fed a macrobiotic diet in early life. *J Bone Miner Res* **12**, 1486–1494.
- Raikow RJ** (1970) Evolution of diving adaptations in the stiff-tailed ducks. *Univ Cal Publ Zool* **94**, 1–52.
- Rajagopalan S, Lu L, Yaszemski MJ, Robb RA** (2005) Optimal segmentation of microcomputed tomographic images of porous tissue-engineering scaffolds. *J Biomed Mater Res A* **75**, 877–887.
- Ridler TW, Calvard S** (1978) Picture thresholding using an iterative selection method. *IEEE Trans Syst Man Cybernet SMC-8*, 630–632.
- Rogers RR, LaBarbara M** (1993) Contribution of internal bony trabeculae to the mechanical properties of the humerus of the pigeon (*Columba livia*). *J Zool Lond* **230**, 433–441.
- Rüeggsegger P, Koller B, Müller R** (1996) A microtomographic system for the nondestructive evaluation of bone architecture. *Calcif Tissue Int* **58**, 24–29.
- Ryan TM, Ketcham RA** (2002a) The three-dimensional structure of trabecular bone in the femoral head of strepsirhine primates. *J Human Evol* **43**, 1–26.
- Ryan TM, Ketcham RA** (2002b) Femoral head trabecular bone structure in two omomyid primates. *J Hum Evol* **43**, 241–263.
- Ryan TM, Ketcham RA** (2005) Angular orientation of trabecular bone in the femoral head and its relationship to hip joint loads in leaping primates. *J Morph* **265**, 249–263.
- Ryan TM, van Rietbergen B** (2005) Mechanical significance of femoral head trabecular bone structure in *Loris* and *Galago* evaluated using micromechanical finite element models. *Am J Phys Anthropol* **126**, 82–96.
- Silva MJ, Keaveny TM, Hayes WC** (1997) Load sharing between the shell and centrum in the lumbar vertebral body. *Spine* **22**, 140–150.
- Swartz SM, Parker A, Huo C** (1998) Theoretical and empirical scaling patterns and topological homology in bone trabeculae. *J Exp Biol* **201**, 573–590.
- Tanck E, Homminga J, Van Lenthe GH, Huiskes R** (2001) Increase in bone volume fraction precedes architectural adaptation in growing bone. *Bone* **28**, 650–654.
- Trussell HJ** (1979) Comments on 'Picture Thresholding Using an Iterative Selection Method'. *IEEE Trans Syst Man Cybernet SMC-9*, 311.
- Underwood EE** (1970) *Quantitative Stereology*. Reading, MA: Addison-Wesley Publishing Co.
- Van Rietbergen B, Muller R, Ulrich D, Rueggsegger P, Huiskes R** (1999) Tissue stresses and strain in trabeculae of a canine proximal femur can be quantified from computer reconstructions. *J Biomech* **32**, 443–451.
- Van Rietbergen B, Huiskes R, Eckstein F, Rueggsegger P** (2003) Trabecular bone tissue strains in the healthy and osteoporotic human femur. *J Bone Miner Res* **18**, 1781–1788.
- Wall WP** (1983) The correlation between high limb-bone density and aquatic habits in recent mammals. *J Paleont* **57**, 197–207.
- Weaver JK, Chalmers J** (1966) Cancellous bone: its strength and changes with aging and an evaluation of some methods for measuring its mineral content. *J Bone Joint Surg* **48-A**, 289–308.
- Weibel ER** (1979) *Stereological Methods*. New York: Academic Press.
- Weibel ER** (1980) *Stereological Methods*. New York: Academic Press.
- Whitehouse WJ** (1974) The quantitative morphology of anisotropic trabecular bone. *J Microsc* **101**, 153–168.
- Whitehouse WJ, Dyson ED** (1974) Scanning electron microscope studies of trabecular bone in the proximal end of the human femur. *J Anat* **118**, 417–444.
- Wilson S, Thorp BH** (1998) Estrogen and cancellous bone loss in the fowl. *Calcif Tissue Int* **62**, 506–511.
- Wolschrijn CF, Weijs WA** (2004) Development of the trabecular structure within the ulnar medial coronoid process of young dogs. *Anat Rec A Discov Mol Cell Evol Biol* **278**, 514–519.

# Author Query Form

---

**Journal: Journal of Anatomy**

**Article: joa\_749.fm**

Dear Author,

During the copy-editing of your paper, the following queries arose. Please respond to these by marking up your proofs with the necessary changes/additions. Please write your answers on the query sheet if there is insufficient space on the page proofs. Please write clearly and follow the conventions shown on the attached corrections sheet. If returning the proof by fax do not write too close to the paper's edge. Please remember that illegible mark-ups may delay publication.

Many thanks for your assistance.

No.	Query	Remarks
1	<b>Laib et al. 2000</b> has been changed to <b>Laib 2000</b> so that this citation matches the list	
2	<b>conflate</b> sense here OK?	
3	<b>Glatt V, Bouxsein ML (in press)</b> please confirm that this has been accepted for publication	
4	<b>eds Gill AP</b> please confirm all Editors, and give chapter page range	
5	<b>Weibel ER (1980)</b> 2 <sup>nd</sup> edn?	

# MARKED PROOF

## Please correct and return this set

Please use the proof correction marks shown below for all alterations and corrections. If you wish to return your proof by fax you should ensure that all amendments are written clearly in dark ink and are made well within the page margins.

<i>Instruction to printer</i>	<i>Textual mark</i>	<i>Marginal mark</i>
Leave unchanged	... under matter to remain	Ⓟ
Insert in text the matter indicated in the margin	∧	New matter followed by ∧ or ∧ <sup>Ⓢ</sup>
Delete	/ through single character, rule or underline or ┌───┐ through all characters to be deleted	Ⓞ or Ⓞ <sup>Ⓢ</sup>
Substitute character or substitute part of one or more word(s)	/ through letter or ┌───┐ through characters	new character / or new characters /
Change to italics	— under matter to be changed	↙
Change to capitals	≡ under matter to be changed	≡
Change to small capitals	≡ under matter to be changed	≡
Change to bold type	~ under matter to be changed	~
Change to bold italic	≈ under matter to be changed	≈
Change to lower case	Encircle matter to be changed	≡
Change italic to upright type	(As above)	⊕
Change bold to non-bold type	(As above)	⊖
Insert 'superior' character	/ through character or ∧ where required	Υ or Υ under character e.g. Υ or Υ
Insert 'inferior' character	(As above)	∧ over character e.g. ∧
Insert full stop	(As above)	⊙
Insert comma	(As above)	,
Insert single quotation marks	(As above)	ʹ or ʸ and/or ʹ or ʸ
Insert double quotation marks	(As above)	“ or ” and/or ” or ”
Insert hyphen	(As above)	⊥
Start new paragraph	┌	┌
No new paragraph	┐	┐
Transpose	└┐	└┐
Close up	linking ○ characters	○
Insert or substitute space between characters or words	/ through character or ∧ where required	Υ
Reduce space between characters or words		↑